NeuroImage: Clinical 2 (2013) 620–629

Contents lists available at ScienceDirect

NeuroImage: Clinical

journal homepage: www.elsevier.com/locate/ynicl

Identification of promethazine as an amyloid-binding molecule using a fluorescence high-throughput assay and MALDI imaging mass spectrometry ☆

Richard A. McClure [a,b,i], Chad W. Chumbley [c,d], Michelle L. Reyzer [d,e], Kevin Wilson [a,b], Richard M. Caprioli [c,d,e,f], John C. Gore [a,b,f,g], Wellington Pham [a,b,f,h,i,*]

[a] Institute of Imaging Science, Vanderbilt University, 1161, 21st Avenue South, Nashville, TN 37232, USA
[b] Department of Radiology and Radiological Sciences, Vanderbilt School of Medicine, USA
[c] Department of Chemistry, Vanderbilt University, USA
[d] Mass Spectrometry Research Center, Vanderbilt University, USA
[e] Department of Biochemistry, Vanderbilt University, USA
[f] Vanderbilt Ingram Cancer Center, Vanderbilt University, USA
[g] Molecular Physiology and Biophysics, Vanderbilt University, USA
[h] Vanderbilt Institute of Chemical Biology, USA
[i] Vanderbilt Brain Institute, USA

ARTICLE INFO

Article history:
Received 19 March 2013
Received in revised form 19 April 2013
Accepted 22 April 2013
Available online 30 April 2013

Keywords:
Alzheimer's disease
Neuroimaging
Promethazine
Amyloid plaques
MALDI-IMS

ABSTRACT

The identification of amyloid-binding compounds is a crucial step in the development of imaging probes and therapeutics for the detection and cure of Alzheimer's disease. Unfortunately, the process typically lags during the translation from in vitro to in vivo studies due to the impenetrable nature of the blood brain barrier (BBB). Here, we integrate fluorescence assay with MALDI imaging mass spectrometry to screen known compounds and repurpose their properties to enable the second function of binding to amyloid plaques. Through this approach, we identified an antihistamine compound, promethazine, that can bind to amyloid plaques. Finally, we demonstrate that promethazine is retained in the amyloid-burdened brain compared to a normal brain and that its distribution within the brain corroborates with that of amyloid plaques.

1. Introduction

Alzheimer's disease (AD) is an age-dependent neurodegenerative disorder characterized by a progressive loss of cognitive function with initial deficits in short-term memory and episodic memory losses followed by increasingly global losses in cognitive function and ultimately death (Artero and Ritchie, 2003). Today, AD represents 50–70% of the cases of senile dementia and remains the only top ten cause of death in the United States without a treatment which directly targets the underlying disease pathophysiology (Aisen, 2008; Terry and Katzman, 1983). To place these statistics in perspective, more than 5 million Americans suffer from this disease, while more than 35 million people are afflicted worldwide (Prince et al., 2011). As a consequence of the baby-boom generation reaching AD's age of onset in congruence with the demographic aging in developing nations worldwide, the future of AD is becoming increasingly daunting with its prevalence projected to reach 65.7 million people by 2030 (Association, 2012). In view of the growing socioeconomic catastrophe and worldwide health problems associated with AD, the impetus to develop new diagnostic and treatment strategies for AD has never been greater.

Currently, in accordance with the amyloid cascade hypothesis of AD pathogenesis, multiple lines of convergent evidence implicate amyloid-β (Aβ) plaques as the major cytopathologic hallmark of AD (Glenner and Wong, 2012; Hardy and Higgins, 1992; Masters et al., 1985a; Selkoe, 1991a,b). The amyloid cascade hypothesis holds that perturbations in Aβ peptide formation and clearance result in a clustering of Aβ peptides to form Aβ plaques, which subsequently cause neuronal death attributable to direct and indirect neurotoxic insults (Lewis et al., 2001; Markesbery, 1999; Meda et al., 1995; Sheng et al., 1997). At present, the diagnosis of AD is assigned clinically by assessing a patient's late-stage cognitive abilities in the context of age, family history and other risk factors (Hintersteiner et al., 2005; Hort et al., 2010; Sorbi et al., 2012). However, due to the phenotypic homogeneity of neurological disorders included in the differential diagnosis of cognitive impairment as well as atypical presentations both intrinsic to AD and secondary to

* Corresponding author at: 1161, 21st Avenue South, Nashville, TN 37027-2300, USA. Tel.: +1 615 936 7621; fax: +1 615 322 0734.
E-mail address: wellington.pham@vanderbilt.edu (W. Pham).

2213-1582/$ – see front matter © 2013 The Authors. Published by Elsevier Inc. All rights reserved.
http://dx.doi.org/10.1016/j.nicl.2013.04.015

confounding morbidities, accurately differentiating AD from non-Aβ causes of dementia remains a bottleneck with respect to both clinical therapeutics and basic research (Albert et al., 2011; Artero et al., 2003; Hardy and Selkoe, 2002; Landau et al., 2011, 2012; Petersen et al., 2001; Ritchie et al., 2010; Van Heertum and Tikofsky, 2003). Critically, studies have demonstrated that AD pathogenesis follows a temporally rapid and predictable course with respect to the regional distribution of Aβ plaque deposition in the brain (Braak and Braak, 1995). Thus, diagnostic strategies targeting Aβ plaques gain a key advantage over other AD biomarkers in that our ability to detect subtle changes in Aβ deposition is the greatest in the regions that change early in the course of AD pathogenesis. Unfortunately, once considerable plaque deposition has occurred, treatments aimed at abolishing these protein aggregations have limited efficacy with respect to restoration of cognitive function, largely as a consequence of the irreversible nature of neuronal damage. Therefore, because neuronal damage cannot be ameliorated, early AD diagnosis and prevention are of paramount importance in the management of AD, as this treatment paradigm likely represents our best hope of curtailing disease burden. Despite the discovery of potentially efficacious therapeutic approaches, the clinical impact of AD treatments remains underwhelming, due in part to a lack of reliable methodologies by which to screen for AD pathology (Aisen and Vellas, 2013; Delrieu et al., 2012; Lansbury, 2004; Merlini and Bellotti, 2003; Rosenberg, 2005).

Of the early diagnostic modalities proposed for AD, amyloid imaging has emerged as the most promising approach with respect to developing a noninvasive yet clinically relevant diagnostic methodology (Cummings and Cotman, 1995; Cummings et al., 1996; de Souza et al., 2012; Perrin et al., 2009; Risacher and Saykin, 2013; Weiner et al., 2012). Today, the most cited modalities in the field of amyloid imaging include optical, MRI and PET-based approaches. For example, optical imaging has been used to monitor the development of a single Aβ plaque and reveal subtle neurite geometry changes that occur in and around diffuse plaques (D'Amore et al., 2003). Similarly, while structural MRI provides exquisite anatomical contrast due to its high spatial resolution, functional and volumetric MRI have also been utilized to predict AD onset with nearly 80% accuracy (Jack et al., 1999; Kerchner, 2011; Koffie et al., 2011; Wang et al., 2006; Yanagisawa et al., 2011). Nevertheless, despite the potential advantages offered by MRI and other optical-based methodologies, PET/CT imaging is still considered the most practical approach because of its sensitivity, detection depth and the ability of PET probes to retain binding affinity for neuroimaging of Aβ plaques (Cohen et al., 2012; Ikonomovic et al., 2012). Despite the real-world availability of PET/CT, amyloid imaging facilitated by this technique is currently limited by the scarcity of specific molecular probes capable of binding to Aβ plaques. Today, the few probes available for PET-based human amyloid imaging include ^{18}F-BAY94-9172 (18F AV-1) (O'Keefe et al., 2009), ^{18}FAV-45 also known as ^{18}F-Florbetapir (Choi et al., 2009), ^{18}F-Florbetaben (Villemagne et al., 2011) and ^{11}C-PIB compounds (Klunk et al., 2004, 2007; Mathis et al., 2012; Mintun et al., 2006). When ^{18}F-Florbetapir was utilized in a well-controlled, randomized study estimating the accuracy of AD diagnosis with and without the assistance of amyloid imaging, diagnostic confidence increased by approximately 21.6%, and 54.6% of clinically based diagnoses were overturned (Grundman et al., 2013). Similarly, a meta-analysis of randomized, controlled trials evaluating the diagnostic efficacy of ^{11}C-PIB estimated its sensitivity and specificity at 93.5% and 56.2%, respectively (Zhang et al., 2012). To date, these compounds have been developed using structural similarity approaches based on the chemical structure of thioflavin or congo red fluorescence dyes (Mathis et al., 2012). However, this deductive approach restricts the ability to select a large number of unorthodox compounds available from a screening library that may bind not only to Aβ plaques, but also encompass other criteria such as the ability to cross the blood brain barrier (BBB). In general, the notable paucity of Aβ binding probes results from the absence of a reliable, high-throughput screening assay capable of identifying novel compounds that bind to Aβ plaques.

Here, we demonstrate a combinatorial approach which integrates a newly designed, high-throughput amyloid thioflavin competitive binding optical assay (HATCO) with matrix-assisted laser desorption/ionization imaging mass spectrometry (MALDI IMS) to facilitate the screening of diverse compound libraries for molecules that possess the ability to bind to Aβ plaques. The HATCO technique provides a robust means of improving the chance for a hit in two distinct ways: first by facilitating the rapid screening of large compound libraries, and second by removing the intrinsic limitations associated with a thioflavin-analog-based probe design. Subsequent utilization of MALDI IMS further expedites the probe design process by obviating investments associated with radiolabeling potential hits discovered in the high-throughput screening phase of our approach. Furthermore, MALDI IMS provides complementary data unobtainable via independent implementation of the HATCO assay by facilitating the direct analysis of intact tissue and preserving the spatial distribution of molecules within that tissue. Thus, MALDI IMS-based analysis of HATCO-discovered hits enables researchers to assess the biological relevance of the molecule's retention pattern in the brain via comparison with known regions of Aβ plaque distribution (Seeley and Caprioli, 2008). To demonstrate the utility of our combinatorial approach to amyloid probe development, we identified promethazine as a potential agent for amyloid imaging among a small library of HATCO-screened compounds (Fig. 1). Adding promethazine to a mixture of freshly isolated and homogenized 5XFAD mouse brain and thioflavin resulted in a significant attenuation of the fluorescence signal, which suggests the compound competes with amyloid-binding thioflavin. Administration of promethazine via tail vein injection into 5XFAD transgenic mice overexpressed with human APP and PS1 resulted in a significantly greater promethazine signal in amyloid-burdened 5XFAD brains compared to wild-type (WT) mice as detected by MALDI IMS. Lastly, the colocalization of promethazine signal in the 5XFAD mouse model with the signal produced by the $A\beta_{40}$ peptide further suggests the interaction of promethazine with amyloid plaques.

2. Materials and methods

2.1. Reagents and mouse model

Thioflavin, naltrexone, and all other chemicals and solvents including methanol, DMSO, and DMF were obtained from Sigma-Aldrich at reagent grade. All chemicals were used without further purification. The absorption spectra were measured on a UV–Vis spectrophotometer (Agilent). Fluorescent measurements were made using a QM-4SE spectrofluorometer (Photon Technology International). The 5XFAD mice were obtained from Jackson Laboratory (Bar Harbor, ME). This APP/PS1 double transgenic mouse model was developed by Vassar et al. (Oakley et al., 2006).

2.2. Animals and brain perfusion

5XFAD and WT mice of different ages were obtained from the in-house Vanderbilt breeding facility and housed in a temperature controlled, 12-hour light/dark cycle facility. After injection of the tested compounds (25 mg/kg), at a designated time point, including 10 min and 4 h, cardiac perfusion was performed. A sharp incision into the abdomen of the anesthetized mouse was made. This was followed by a longitudinal cut with a scalpel to open the thoracic cavity, which then was stabilized with a retractor. Perfusion began with a 20-gauge syringe containing ice cold PBS (30 ml, pH 7.4) in the left ventricle while the atrium was snipped followed by the injection of paraformaldehyde (PFA) solution (4%). Once the perfusion was completed, the animals were decapitated and the brains were quickly removed and fixed in PFA overnight at 4 °C followed by sucrose precipitation overnight at 4 °C. The brains were then embedded in Cryo-OCT compound (Fisher Scientific) before sectioning. All animal experiments performed complied with institutional guidelines and were conducted according to the protocol approved by the Vanderbilt Institutional Animal Care and Use Committee.

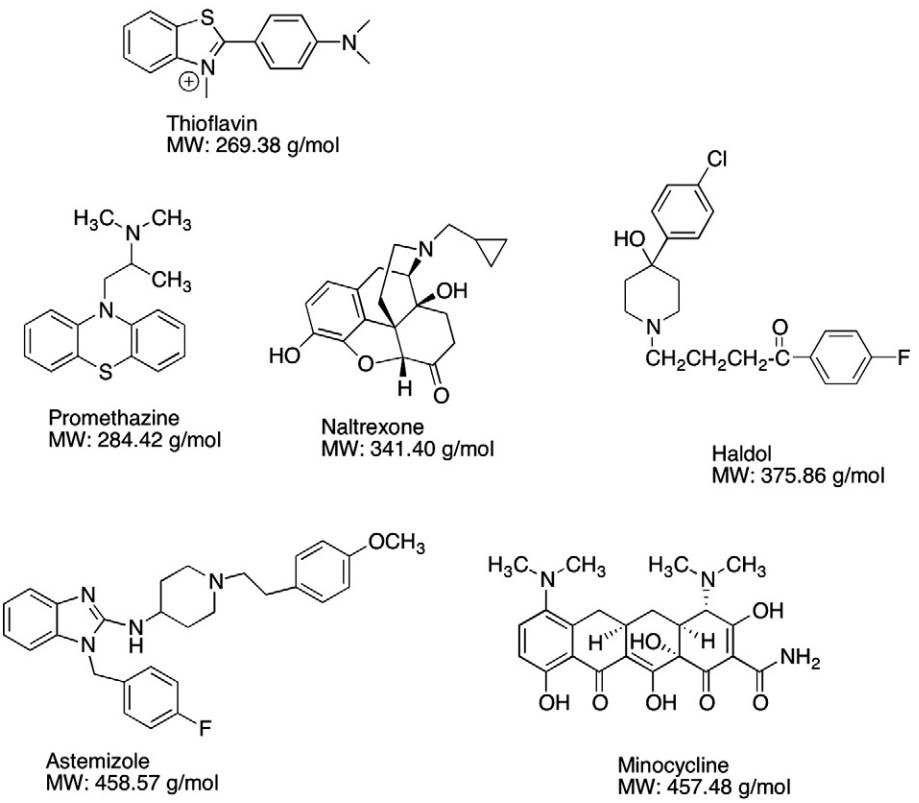

Fig. 1. Chemical structures and molecular weights of thioflavin and candidate amyloid-binding compounds. Thioflavin and a series of selected compounds comprising a small molecular library were screened for the ability to bind Aβ plaques using the HATCO assay. Structural diversity was maximized within this library to include benzimidazole, benzylisoquinoline, butyrophenone, tetracycline and phenothiazine motifs contributed by astemizole, naltrexone, haloperidol, minocycline, and promethazine, respectively.

2.3. HATCO assay

Thioflavin stock solutions were prepared by dissolving 1.3 mg in 100 mL of dd. water. The solution was passed through a micro filter after which the concentration was measured using Beer's law using an extinction coefficient of 26,620 M^{-1} cm^{-1} at 416 nm. The stock solution was stored in darkness using aluminum foil and kept at 4 °C during the assay. Fresh stock solution was prepared for each assay. Fluorescence was measured using excitation/emission parameters at 465/565 nm with 5 nm slits, 0.1 second integration time and at 1-nm intervals using a Photon International fluorometer. In a typical measurement, thioflavin (50 μL, 40 μM) was added to 100 μL of freshly prepared and vortexed 5XFAD amyloid lysate (70 mg/mL). The mixture was incubated at room temperature for 10 min. After incubation, test compounds (50 μL) in PBS (50 mM) were added to the mixture. The concentration of the tested compounds was 250 μM. After equilibration for 10 min at room temperature, the fluorescence signal of the sample was measured at an emission lambda max of 480 nm. All measurements were performed in triplicate and data are presented as mean with standard deviation.

2.4. Thioflavin fluorescence staining

Cryostat prepared coronal midbrain slides (8–12 μm thickness) were mounted and fixed using PFA. The slides were stored at −80 °C until use. Before staining, slides were thawed and placed in 4% PFA for 10 min before being transferred to TRIS buffer for 5 min and dried before exposure to the thioflavin solution (1% dye content). The stained slides were maintained at 37 °C for 30 min after which the excess thioflavin was removed prior to rinsing in the TRIS buffer for 1 min. The slides were then dipped into 95% ethanol followed by 100% ethanol for 6 s. They were then allowed to air dry at room temperature. Coverslips were added to slides using Vecta shield mounting solution and allowed to dry overnight prior to fluorescence microscopy using DAPI filter channel.

2.5. Quantification of the uptake by HPLC

Whole brains from perfused 5XFAD or WT mice treated previously with promethazine at different times were collected, weighed, and homogenized in PBS (g tissue/3 mL PBS) using a homogenizer (Tissuemizer Homogenizer, Fisher Scientific, Pittsburg, PA). The homogenized solution was added with 20% acetonitrile and warmed at 70 °C using a heating block for 10 min to maximize promethazine extraction. The extract was lyophilized and then reconstituted with HPLC buffers. After establishing the detection limit of the instrument and determining a promethazine concentration–response calibration curve, the quantitative amount of promethazine in the brain lysate against the injected dose was analyzed by integrating the area under the curve using EZChrome Elite software (Hitachi). Every retention time peak in the spectrum was collected and analyzed using LC–MS.

2.6. Amyloid lysate preparation

Excised midbrains were homogenized for 5 min in 200 μL of buffer comprised of 21.4 g sucrose, 5 mL of 1 M tris base, and 0.5 mL of 0.5 M EDTA/250 mL DPBS using the T-25 basic Ultra-Turrax homogenizer. Additional 100 μL aliquots of this buffer were then added to the homogenized sample and re-homogenized for 2 min until a total added volume of 800 μL was attained. The sample was diluted to 4 mL total volume using another buffer comprised of 5% BSA, and 0.03% Tween 20 in DPBS solution. Roche Complete protease inhibitor tablets were added to both buffers immediately prior to use (1 tablet/10 mL

buffer). The sample was centrifuged at 16,000 *g* for 30 min at 4 °C. Aliquots of the supernatant were stored at −80 °C until use.

2.7. MALDI IMS imaging

Analyse of promethazine were performed on an LTQ XL linear ion trap mass spectrometer equipped with a MALDI source (ThermoFisher, Waltham, MA). Fresh frozen mouse brain coronal sections of 12 μm were thaw-mounted onto gold-coated, stainless steel target plates which were kept at room temperature in a vacuum desiccator until analysis. A serial section was obtained on a glass slide and stained using hematoxylin and eosin. The tissue sections were manually coated with matrix (DHB, 30 mg/mL in 50:50 methanol:water with 0.1% trifluoroacetic acid) using a glass nebulizer (thin-layer chromatography reagent sprayer, Kontes Glass Company, Vinland, NJ). The matrix was applied by passing the sprayer across the tissue section several times and allowing the tissue to dry. This process was repeated approximately 20 times to ensure a homogeneous coating of matrix crystals formed on the tissue section while minimizing analyte delocalization. After coating, the target plate was attached to a modified LTQ slide holder and inserted into the instrument. MS/MS spectra for promethazine were acquired over the entire tissue section at 100 μm spatial resolution. An isolation window (1.0 amu) centered on *m/z* 285 was selected to isolate the precursor ion for PMZ. This was subjected to collisionally activated dissociation (CAD) at a collision energy of 27. Main fragment ions were formed at *m/z* 86 and 198 (likely corresponding to fragmentation at the phenothiazine-*N*) as well as at *m/z* 240 (likely corresponding to loss of the dimethylamine moiety) (Niessen, 2011). Images representative of the distribution of PMZ across the tissue section were generated by plotting the summed intensity of the main fragment ions at *m/z* 86 and 240 at each pixel using ImageQuest software (Thermo Scientific, Waltham, MA). Analyses of amyloid peptides were performed on a linear MALDI time-of-flight mass spectrometer (Autoflex, Bruker Daltonics, Billerica, MA). The samples on the plate analyzed using the LTQ were washed in sequential steps of 70% ethanol, 100% ethanol, Carnoy's solution (60% ethanol, 30% chloroform, 10% acetic acid), and water to remove the matrix and potential ion suppressant's such as lipids and salts. After reapplying the matrix, three brain sections were imaged in positive ion mode from *m/z* 2500–7000 at a spatial resolution of 75 μm. Specific ion images were reconstructed in fleximaging software (Bruker Daltonics, Billerica, MA).

2.8. Image analysis

Each coronal brain slice was manually segmented to create individual ROIs of the hippocampus and isocortex or of the whole coronal section. The Allen mouse brain atlas was used as a reference for the segmentation of these regions and analysis was performed by an outside collaborator. The ROIs were then used to isolate the pixels in the MALDI ion images representing promethazine (*m/z* 86 + 240) and the pixels within the direct $A\beta_{40}$ images (*m/z* 4331 +/− 4). Once the images were segmented, mean signal values were calculated (Fig. 5B). Next, the pixels within each ROI were segmented into two groups using the k-means clustering algorithm, which represents signal vs. no signal. The comparison of these measurements is shown in Fig. 5C.

3. Results

3.1. HATCO assay-mediated screening for novel Aβ-binding compounds

Thioflavin is classified as a topologically activated dye that binds specifically to Aβ plaques (Nolting et al., 2011). This class of compounds possesses substantial conformational freedom while remaining in free solution and thus exhibits a relatively low fluorescence signal. However, upon binding to Aβ plaques, thioflavin's conformational freedom is dramatically reduced. This increase in structural rigidity decreases the vibrational–rotational processes available to the thioflavin molecule, resulting in a decreased radiation decay rate of thioflavin in both ground and excited states. Cumulatively, these phenomena contribute to the observed increase in thioflavin's fluorescence quantum yield when bound to Aβ plaque compared to the unbound molecule (Nesterov et al., 2005; Voropai et al., 2003). Although increased thioflavin fluorescence alone is highly indicative of the thioflavin molecule existing in an Aβ-bound state, secondary validation of this fact is available as a consequence of a characteristic spectral shift in thioflavin's fluorescence signal observed only when thioflavin is bound to Aβ plaques. As discussed, when not complexed with Aβ, thioflavin emits a weak fluorescent signal at a λ_{max} of 440–445 nm. However, when bound to Aβ plaques, thioflavin's fluorescence increases dramatically resulting in a strong fluorescent signal with a characteristically shifted λ_{max} of approximately 480 nm (Hudson et al., 2009; LeVine, 1993). We employed these unique characteristics of thioflavin to develop the HATCO assay for screening compounds for the ability to bind to Aβ plaques in a high-throughput fashion. In an effort to utilize the most biologically representative Aβ plaques possible, fresh brain lysates were obtained from 5XFAD mice and analyzed using the Bradford assay to ensure an equal amount of protein was used in each assay trial. Before performing a specific displacement study, we conducted a series of control experiments intended to (i) assess whether the tested library of compounds emitted or absorbed at wavelengths might confound thioflavin's signal by overlapping with its excitation or emission spectra and (ii) demonstrate the specificity of thioflavin toward Aβ plaques. As shown in Fig. 2A, when the compounds were mixed with thioflavin in the absence of Aβ plaque, no significant modulation of thioflavin fluorescence is observed. These findings lend strong support to the claim that the compounds tested do not bind to thioflavin directly and are incapable of directly modulating its fluorescence due to overlapping spectra. In support of thioflavin's affinity for Aβ plaques, mixing thioflavin (10 μM) with Aβ plaques (35 mg/mL) contained within the 5XFAD brain lysate resulted in a nearly 19-fold enhancement in thioflavin fluorescence signal compared to a control sample ($P < 0.0001$) in which the same concentration of thioflavin was dissolved in PBS without Aβ protein. Importantly, the enhanced fluorescence signal of thioflavin observed in the presence of the 5XFAD lysate exhibited a λ_{max} of 480 nm, a characteristic of thioflavin bound to Aβ plaques. By comparison, the thioflavin mixed with PBS controls emitted most strongly at 440 nm, which is the λ_{max} associated with unbound thioflavin. In a more rigorous demonstration of thioflavin's specificity for 5XFAD-derived Aβ plaques, we treated the same thioflavin concentration with brain lysate isolated from WT mice lacking Aβ plaques. Despite some degree of non-specific binding, a reliable differential in fluorescence signal enhancement was observed between amyloid-containing 5XFAD lysate and amyloid-deficient WT lysate, which confirmed our hypothesis that thioflavin fluorescence could be used as a reliable reporter to identify Aβ-binding compounds. Again, spectral analysis of thioflavin's fluorescence in the presence of WT lysate reveals a λ_{max} of 440 nm as compared to the λ_{max} of 480 nm observed in the 5XFAD trials. This spectral shift confirms the thioflavin fluorescence signal utilized as a reporter in the subsequent HATCO assays reliably reflects the proportion of Aβ-bound thioflavin. Thus, any observed modulation in thioflavin fluorescence when the compounds are added cannot represent the dissociation of thioflavin from non-Aβ proteins, as these complexes do not contribute to the measured thioflavin signal at 480 nm (Fig. 2B).

Next, we tested the ability of the compounds to displace thioflavin for binding to Aβ plaques. Again, the assumption was that if thioflavin is dissociated from Aβ plaques by a competitively binding compound, the fluorescence signal of thioflavin would be reduced. 5XFAD brain lysates of normalized concentration were treated with thioflavin in quartz cuvettes and allowed to equilibrate for 30 min before the addition of the tested library compounds. After equilibration, the proportion of thioflavin molecules bound to Aβ plaques in solution was

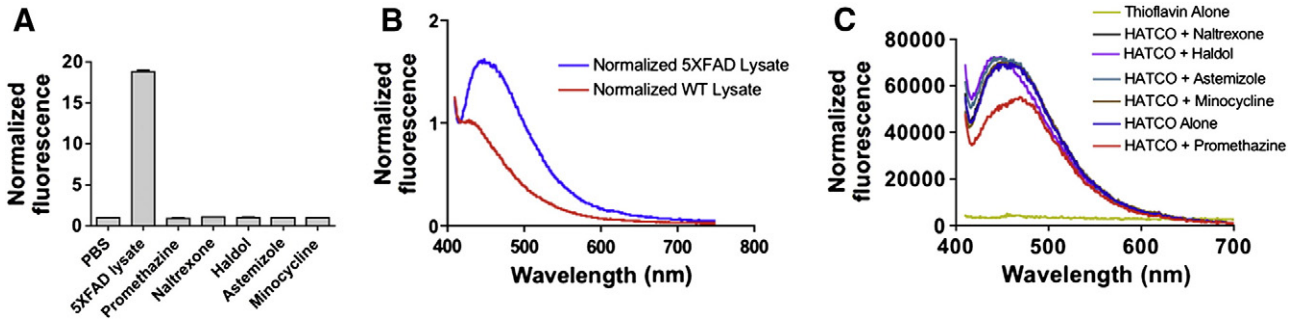

Fig. 2. HATCO assay-mediated, high-throughput screening of structurally diverse compound libraries for Aβ plaque-binding capacity. (A) Fluorescence signal of thioflavin in the presence of freshly isolated 5XFAD brain lysate, PBS or candidate compounds. The results demonstrate a 19-fold increase in thioflavin fluorescence in the presence of 5XFAD lysate compared to PBS and compound library trials ($P < 0.0001$). Values represent normalized fluorescence with respect to PBS trial ± S.D. (n = 3). (B) Enhancement of thioflavin fluorescence in the presence of 5XFAD lysate compared to WT lysate. The spectral shift in thioflavin's λ_{max} toward 480 nm in the presence of 5XFAD lysate arises as a consequence of thioflavin-amyloid complexes and validates the reliability and specificity of the thioflavin reporter. Note that the emission maximum of 440 nm in the WT trials excludes the possibility of the thioflavin signal enhancements representing non-specific binding of thioflavin to endogenous peptides of the brain. Protein concentrations in 5XFAD and WT lysates were normalized throughout the assays. (C) Increased thioflavin fluorescence secondary to the presence of amyloid-containing 5XFAD lysate is attenuated by the addition of promethazine but not by other candidate compounds. Promethazine reduces thioflavin fluorescence at 480 nm by 15.6% with respect to PBS trials ($P < 0.0001$). The results suggest promethazine may displace thioflavin for amyloid plaques and thus attenuate the fluorescence signal. All measurements were performed in triplicate at candidate compound concentrations of 250 μM.

measured using fluorescence spectroscopy. Among the tested compounds, we found that only promethazine caused a notable reduction (19%) of thioflavin's fluorescence signal ($P < 0.0001$) (Fig. 2C). Of note, it is improbable that this signal attenuation is attributable to fluorescence resonance energy transfer (FRET), as promethazine is not a chromophore and is therefore unable to interfere with the excitation states of thioflavin via the FRET mechanism.

3.2. Blood brain barrier penetration

The next phase of experiments evaluated promethazine's ability to cross the BBB and be retained in the brain parenchyma in an amyloid-dependent manner. Wild-type and 5XFAD mice (n = 3 per group) were injected with promethazine (25 mg/kg) via the tail veins and subsequently perfused 10 min or 4 h post-injection. Freshly isolated brains were then homogenized to facilitate extraction and quantification of the promethazine contained within the sample via HPLC using a procedure reported by our group previously (Kumagai et al., 2012). As shown in Fig. 3, following a brief systemic distribution, we noted pronounced peaks at retention times of 15 and 17 min, which corresponded to (R) and (S) enantiomers, respectively (Allender and Archer, 1984; Ponder and Stewart, 1995). Of note, the molecular weight of the molecule associated with the peaks at 15 and 17 min match that of promethazine as determined by LC–MS and identically matches the peaks obtained by HPLC analysis of a racemic promethazine solution (data not shown). Among the WT mice, the peaks corresponding to both (R)- and (S)-promethazine disappeared 4 h post-injection. However, both enantiomers of promethazine remained in amyloid-burdened 5XFAD brains 4 h post-injection. Interestingly, retention of the (S)-enantiomer appeared favorable compared to that of the (R) configuration. This may suggest that the (S) configuration of promethazine is principally responsible for binding to Aβ plaques. Using standardized concentration curves and integration software available from the HPLC system, we calculated that 2% and 0.5% of the original promethazine dose was retained 10 min post-injection in 5XFAD and WT mice, respectively. Thus, promethazine exhibits a 4-fold higher retention in amyloid-burdened brains at the 10-minute time-point with respect to WT controls. At the 240-minute time-point, 0.5% of the original dose remained in 5XFAD brains compared to 0.01% retention in the WT animals. These results represent a significant difference in the retention of promethazine as a function of Aβ plaque burden in the brains at the 240-minute time-point. Further analysis of this data reveals that the amount of promethazine retained in the brain of WT mice drops 97% during the 10- to 240-minute time interval, while promethazine retention falls by only 75% in amyloid-burdened 5XFAD brains. We performed a control study to demonstrate the notion that compounds lacking any kind of binding targets in the brain will be virtually 100% cleared an hour after administration. Toward that goal, we injected Cy5.5 succinimide ester dye (2 nmol) into the left ventricle of a mouse and tracked the distribution using an optical imaging system. Immediately after injection, we observed the dye diffused into the brain tissues; however, one hour post-injection, no trace of the material was detected in the brain (Supplementary data, Fig. S1). Thus, the finding that the rate of promethazine clearance in the brain varies in an amyloid-dependent manner is best explained by the ability of the compound to bind to Aβ plaques. Taken together, the data confirm that promethazine can penetrate the BBB and be retained in the brain in an amyloid-dependent manner.

3.3. MALDI IMS ex vivo imaging of promethazine's spatial distribution in the 5XFAD brains

Before analyzing the distribution of promethazine in the brains of treated mice, we optimized the MALDI IMS method for promethazine. Promethazine was analyzed on a linear ion trap equipped with a MALDI source (Thermo LTQ XL), using 2,5-dihydroxybenzoic acid (DHB) as the matrix. Promethazine forms a protonated ion at *m/z* 285.1, which was subjected to collisionally activated dissociation. Fragmentation occurs at the nitrogen moieties, resulting in three main fragment ions including the phenothiazine ring, a substituted N-propyl phenothiazine, and N,N-dimethylisopropylamine at *m/z* 198, 240 and 86, respectively. These ions are unique to promethazine and are not observed in the DHB matrix (Fig. 4A & B).

Next, we determined whether promethazine accumulates sufficiently in the brain to permit detection. Eight-month-old 5XFAD (n = 5) and age-matched WT mice (n = 3) were used to assess the distribution and localization of promethazine in the brain. The animals were injected with promethazine (25 mg/kg) via the tail vein followed by brain perfusion 4 h post-injection. Non-dosed animals were used as controls. After perfusion, the brains were removed and flash frozen. The frozen brains were then sectioned into 12-μm thick slices, coated with DHB, and analyzed on the LTQ via pseudo-selected reaction monitoring (SRM). Fig. 4C shows the detected promethazine signal (from *m/z* 86) on representative brain sections from dosed WT (top), non-dosed 5XFAD (middle), and dosed 5XFAD (bottom) animals. As shown, there is no measurable signal from the non-dosed sample. Promethazine is detected from both dosed animals, but there is a significantly higher signal from the 5XFAD sections. Similar images were obtained for the other

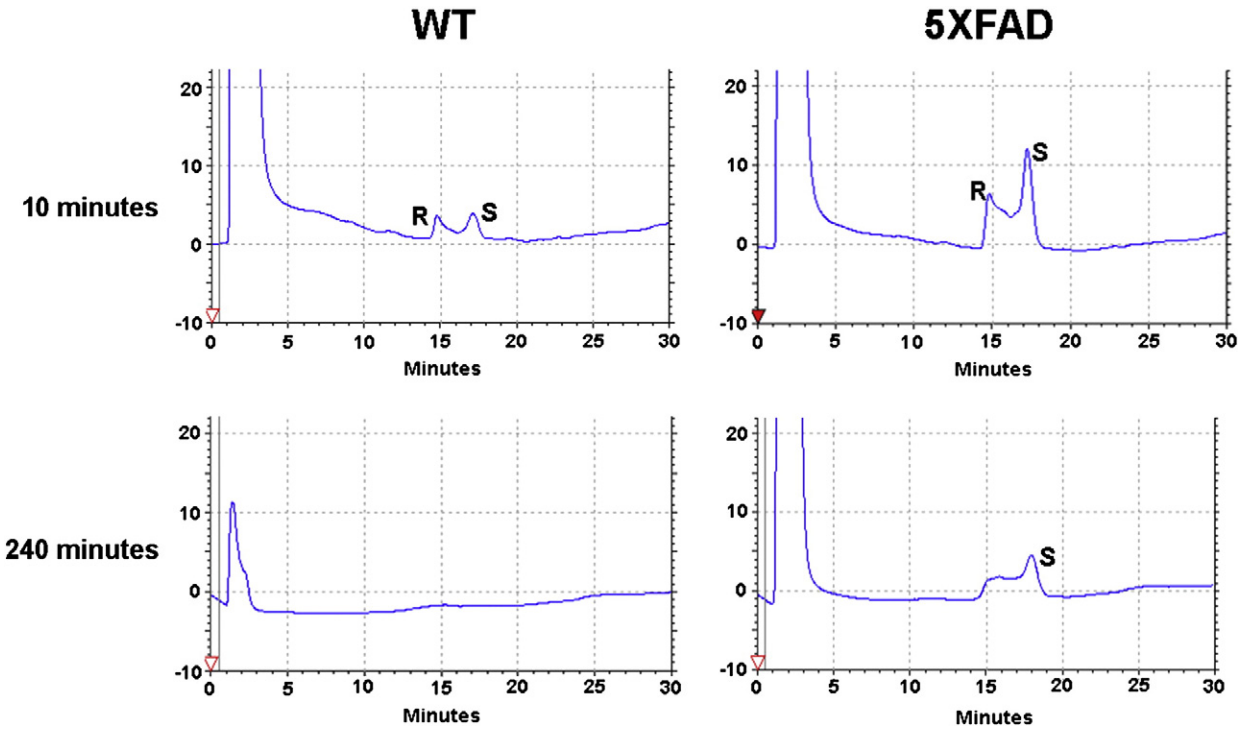

Fig. 3. HPLC determination of BBB penetration and differential retention of (S)-promethazine in 5XFAD mouse model. Ten minutes post-injection, detectable levels of promethazine were measured in both WT (mean = 2.57 μg) and 5XFAD (mean = 9.62 μg) mouse models, thus confirming promethazine's ability to cross the BBB in both models. At this time-point, 0.5% of the original promethazine dose is retained within the brains of WT mice compared to 2% retention in the 5XFAD model. This is approximately a 4-fold increase in promethazine retention in amyloid-burdened brains. At the 240-minute time-point 0.5% of the original dose retained in 5XFAD brains versus 0.01% in WT mice. Given that the difference in promethazine retention between WT and 5XFAD grows over time, it is highly probably the enhanced retention of promethazine in amyloid-burdened brains reflects an affinity of promethazine for Aβ plaques. Tail vein injection of racemic mixtures of promethazine facilitated the determination of stereo-specific binding. Note that both the (R)- and (S)-promethazine enantiomers are retained at relatively the same level in WT brains; however, the (S)-version is retained at higher levels 240 min post-injection in the 5XFAD mice. These results support the conclusion that the (S)-promethazine enantiomer may be primarily responsible for Aβ plaque binding. Further, cardiac perfusion protocol was performed prior to brain extraction/homogenization to avoid confounds associated with promethazine being retained in the micro-vasculature. All measurements were performed in triplicate with each dose equivalent to 25 mg/kg.

two fragment ions (*m/z* 198 and *m/z* 240), confirming the molecular specificity of the analysis.

3.4. Corroboration of promethazine's regional retention with Aβ plaque distribution in the brain using MALDI IMS

In this phase of the study, coronal brain sections from three groups of mice were used to investigate whether the regional distribution of promethazine mirrored that of Aβ plaques. Two-month-old (n = 4) and 8-month-old 5XFAD (n = 4) mice as well as 8-month-old WT mice (n = 4) were dosed with 25 mg/kg of promethazine via tail vein injections. Cardiac perfusion was subsequently performed 4 h after treatment, and the brains were freshly frozen and prepared for MALDI IMS analysis. By employing the MALDI IMS methodology, we were able to determine the regional distribution and relative abundance of promethazine and the $A\beta_{40}$ peptide within a single coronal

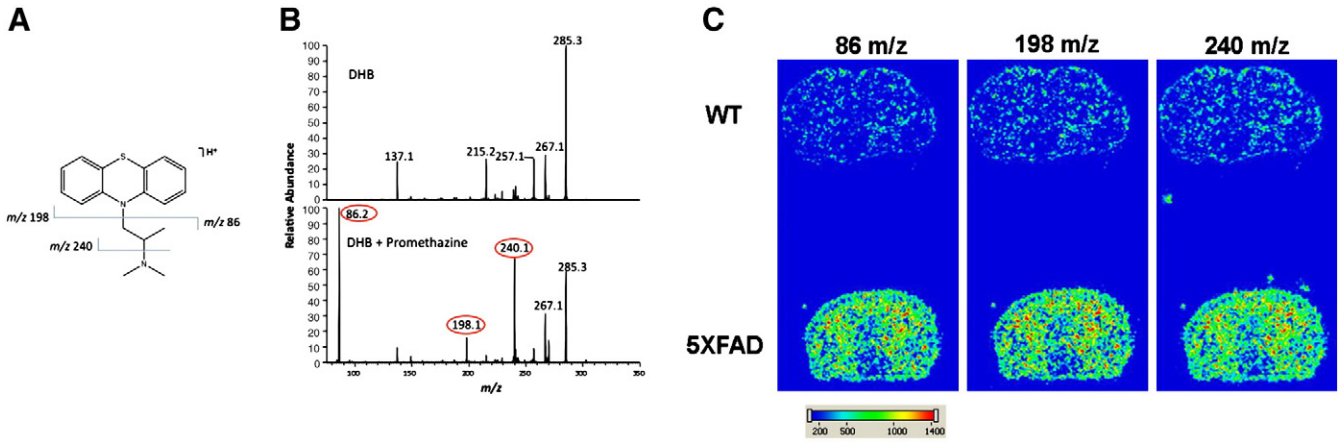

Fig. 4. Validation of promethazine imaging using MALDI IMS. (A) Chemical structure of promethazine and its fragmentation pattern under the described MALDI IMS condition. (B) Fragmentation of promethazine generates ions with unique *m/z* values (red circles) that are distinct from the DHB matrix. (C) Visualization of promethazine retention in 12-μm coronal brain slices of dosed 5XFAD and WT mice at three ions. Mice were given a cumulative dose of 25 mg/kg of promethazine using four tail vein injections at 2-hour intervals. Animals were subsequently sacrificed 3 h following the last injection. Note the enhanced retention of promethazine in amyloid-burdened brain tissue (5XFAD) compared to WT. The high degree of corroboration between all three *m/z* peaks confirms the specificity of this protocol for promethazine (n = 3 per group).

section. Critically, the $A\beta_{40}$ peptide is widely accepted in the field of AD research as a major constituent of mature Aβ plaques, and it has been shown to possess considerable cytotoxicity (Ghiso and Frangione, 2002; Masters et al., 1985b). Thus, our study assumes that $A\beta_{40}$ deposition reasonably reflects the regional Aβ plaque load in any given region of the brain. As illustrated in Fig. 5A, direct imaging of the $A\beta_{40}$ peptide reveals a 5-fold increase in Aβ plaque burden in the 8-month-old 5XFAD cohort as compared to both the 2-month-old 5XFAD animals and age-matched WT controls. Furthermore, critical analysis of these images further reveals a predilection for Aβ plaque deposition in specific regions of the brain including the isocortex and hippocampal CA1–CA3 areas. Interestingly, both the promethazine and $A\beta_{40}$-generated signals measured in the 2-month-old 5XFAD mouse cohort did not differ significantly from those of treated WT brains. This finding is consistent with thioflavin staining, which confirms that Aβ plaques are not well developed at this age (Supplementary data, Fig. S2). In an effort to demonstrate promethazine's potential efficacy as a reporter of Aβ plaque burden in the brain, we first quantified the total promethazine-generated MALDI IMS signal in each of the three cohorts. To do this, we employed standard image processing techniques which rely on transformation of the MALDI IMS data into a binary image format to facilitate quantification of the average signal intensity generated by promethazine and the $A\beta_{40}$ peptide. As depicted in Fig. 5B, MALDI IMS imaging of promethazine in 8-month-old 5XFAD animals revealed a signal intensity nearly 3-fold greater than that of age-matched WT animals. In contrast, promethazine-dosed WT mouse brains exhibit virtually no $A\beta_{40}$-generated signal and a minimal signal representing promethazine. This data is consistent with the HPLC data presented in Fig. 3, which indicates that only residual amounts of promethazine remain in the brain of WT mice 240 min post-injection. Notably, the signal trends observed in promethazine signal mirror those of direct Aβ peptide imaging; as signal intensities derived from both promethazine and the $A\beta_{40}$ peptide are similarly elevated in 8-month-old 5XFAD mice compared to age-matched WT controls. In addition, the level of Aβ plaque burden assessed by MALDI IMS imaging of the $A\beta_{40}$ peptide is comparable within experimental groups, a finding which alludes to the possibility of inter-subject comparisons of Aβ plaque burden using this technique. Lastly, no promethazine-generated signal was detected in non-promethazine-dosed 8-month-old 5XFAD brains ($n = 2$, Supplementary data, Fig. S3), thus excluding the possibility of signal artifacts underlying the observed differences in promethazine retention. However, it remained possible that the brain regions responsible for generating the enhanced promethazine signal in the 8-month-old 5XFAD cohort might not be of biological significance with respect to AD pathophysiology. Therefore, we sought to investigate whether regions of known pathological significance, including the isocortex and hippocampal fields possessed promethazine signal differences like those observed in the whole brain analysis. As depicted in Fig. 5C, quantification of the MALDI IMS signal intensities generated by promethazine within each experimental group supports the conclusion that promethazine is retained as a function of the Aβ plaque burden in regions of the brain relevant to AD pathophysiology. On average, the promethazine signal measured in the brains of 8-month-old 5XFAD mice is 2-fold greater than that of age-matched controls in both the hippocampus and isocortex ($n = 3$ per region, $P < 0.01$). In congruence with our whole brain analysis, no significant differences in promethazine retention were observed between WT and 2-month-old 5XFAD animals in either of these regions. Considered together, the similarity in mean signal values generated by promethazine and $A\beta_{40}$ in each experimental cohort, in addition to the evidence which illustrates that these trends are observable in biologically relevant

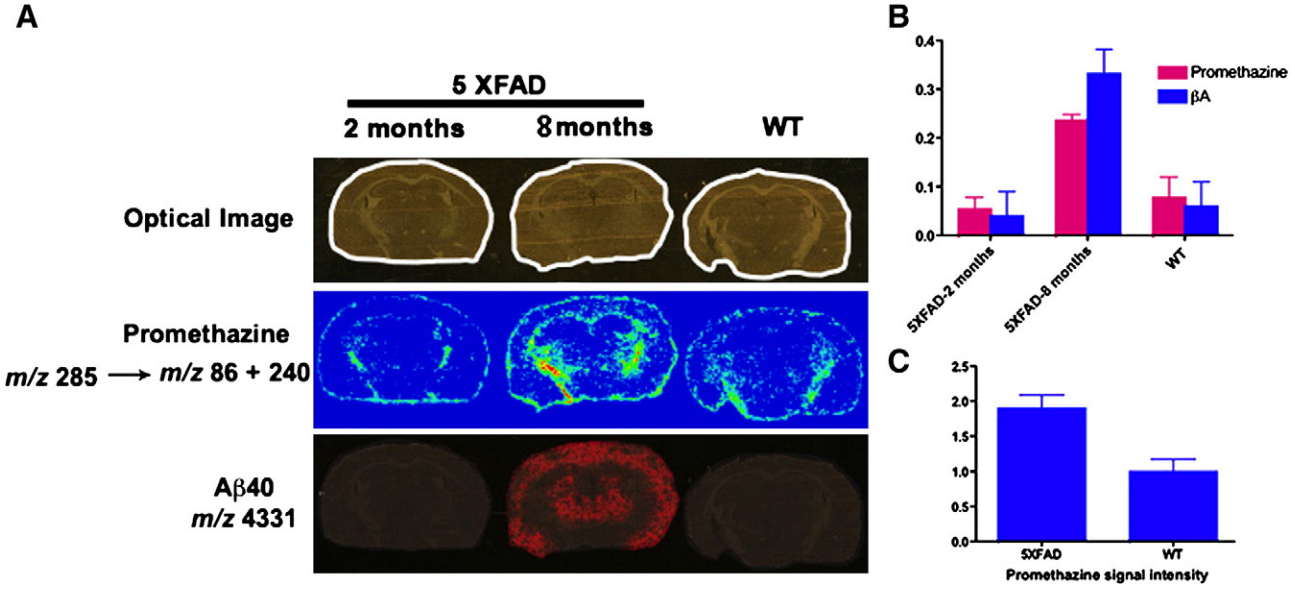

Fig. 5. Differential retention of promethazine as a function of Aβ plaque burden. (A) Representative coronal brain slices obtained from promethazine-treated WT and 5XFAD mice (4 h post injection) were assembled on a gold plate for analysis via MALDI IMS. In the $A\beta_{40}$ imaging panel, the comparable signal intensities in the WT and 2-month-old 5XFAD cohorts implies that Aβ plaques are not well developed in 2-month-old 5XFAD mice. Importantly, this finding excludes differences in BBB permeability or brain protein composition between 5XFAD and WT models as alternative explanations of the differential retention of PMZ observed in the 8-month-old 5XFAD group. The differential signal intensity of PMZ between 2- and 8-month-old 5XFAD mice confirms promethazine's potential to serve as a proxy of Aβ plaque burden as well as demonstrates its specificity for mature Aβ plaques. (B) Quantification of total brain promethazine and $A\beta_{40}$-generated MALDI IMS signal in WT and 5XFAD mice. Signal intensity was calculated as the percentage of pixels exhibiting promethazine-generated MALDI IMS signal above background levels. The mean promethazine-generated MALDI signal obtained from brains of 8-month-old 5XFAD mice was 3-fold greater than that of WT controls ($n = 3$, $P < 0.01$). Furthermore, no significant differences in promethazine-generated signal were observed between 2-month-old 5XFAD mice and WT controls ($P = 0.47$). Critically, these trends in promethazine retention between experimental cohorts directly mirror those observed via direct visualization of the $A\beta_{40}$ peptide, thus supporting the conclusion that promethazine retention in the brain is amyloid dependent. (C) Quantification of promethazine-generated MALDI IMS signal in pathologically relevant regions of interest. Overlay of MALDI IMS promethazine images with the Allen mouse brain reference atlas facilitated quantification of the mean promethazine-generated signal intensities within the hippocampus and isocortex. Mean signal values from these regions were then normalized to age-matched WT controls. Within these regions of interest, promethazine retention was significantly greater in 8-month-old 5XFAD mice compared to WT controls ($n = 3$, $P = 0.006$). The results suggest that promethazine is retained preferentially in amyloid-burdened brains in regions of the brain known to be susceptible to Aβ plaque aggregation.

brain regions, lends convincing support to the conclusion that promethazine is preferentially retained in the brain in an amyloid-dependent manner.

3.5. MALDI IMS for amyloid peptides

The same sections analyzed for promethazine were analyzed for individual amyloid peptides. The sample plate was put into a time-of-flight MS (Bruker Autoflex TOF) and analyzed in linear positive ion mode from *m/z* 2500–7000. A number of signals corresponding to amyloid peptides were detected, as shown in Table 1 (based on human amyloid precursor protein, Swiss Prot entry number P05067). The signal for *m/z* 4332, corresponding to Aβ (1–40) was the most abundant Aβ signal. The localization of *m/z* 4332 is shown in Fig. 5. As shown, the 8-month-old 5XFAD brains show the highest amount of amyloid peptide signal. The resulting image is similar for all amyloid ions detected (data not shown). It is interesting to note that the amount of peptide in the 2-month-old 5XFAD mouse is similar to the 8-month-old WT mouse, supporting the observation from promethazine localization that there is a reduced amount of plaques in the 2-month-old animal. The high amount of Aβ peptide in the 8-month-old 5XFAD mouse brain is consistent with the AD phenotype, and supports the notion that promethazine is accumulating in the brain in the presence of amyloid plaques.

3.6. Statistical analysis

The experimental data were reported as mean ± SD. We compared the test groups using the Mann–Whitney *t*-test using GraphPad software (La Jolla, CA). *P* values are two-tailed and differences with *P* values <0.05 were considered statistically significant.

4. Discussion

Despite the availability of amyloid-binding contrast agents in clinical trials, the development of novel probes remains a significant bottleneck in the overall effort to detect and treat AD. Given the costly development and structural limitations intrinsic to thioflavin analog-based probe design, the impetus for our work is the passion to find new approaches which facilitate the identification of unorthodox, amyloid-binding compounds that can expand and potentially improve upon our current repertoire of amyloid imaging agents. Although current amyloid imaging probes represent a considerable breakthrough in AD research, complete validation of the diagnostic efficacy of these compounds will likely require decades of validation. In this work, we describe a robust, reliable and rational technique for the identification of ideal amyloid-binding compounds. This approach obviates the development of unsuitable compounds and minimizes potentially colossal and wasteful investment associated with traditional probe design strategies. Yet another advantage of this technique is that both the HATCO assay and MALDI IMS are suitable for the high-throughput platform. As demonstrated in this work, the correlation between the candidate compound's topographical brain distribution and that belonging to amyloid peptides can be used to lend biologically relevant support to a compound's ability to serve as a proxy for Aβ plaque burden.

Among the library of compounds tested, promethazine alone attenuated the thioflavin fluorescence signal in the presence of freshly isolated 5XFAD brain lysates. This robust inhibitory profile indicates the possibility of direct displacement of thioflavin by promethazine upon binding to Aβ plaques. This notion is supported by the fact that thioflavin signal enhancement is due to binding Aβ plaques. In support of this conclusion, we have demonstrated that the excitation/emission spectra of thioflavin are not influenced by promethazine. To exclude native brain proteins as sources of the elevated thioflavin fluorescence used as a reporter in these experiments, we demonstrated that the thioflavin signal is not enhanced when exposed to WT mouse brain lysates. Having successfully identified a lead compound for our study, the next task in our approach was to determine whether promethazine could penetrate the BBB. This is an important step in our overarching effort to develop probes suitable for in vivo imaging, as many molecules, including thioflavin are incapable of crossing that barrier. By using a racemic mixture of promethazine for in vivo injection, we demonstrated that promethazine accumulates and is retained briefly in normal brains before being almost completely washed out after 240 min. However, if brains were burdened with a significant Aβ plaque density, the (S)-promethazine is preferentially retained.

Ideal amyloid imaging probes that aim to dramatically impact AD research should demonstrate the potential to detect Aβ plaque expression well beyond the yes/no strategy. Rather, they should move toward the capability of quantitatively evaluating plaque burden in order to facilitate intra-subject longitudinal studies of Aβ plaque load. As Aβ plaque deposition is the hallmark of AD, such an ideal probe would become a tool with which to assess plaque expression levels in response to therapy and provide insight into the observed variability during the course of the disease. Toward that end, 5XFAD and age-matched controls were used for ex vivo MALDI IMS analysis of promethazine retention in the brains. MALDI IMS imaging showed a clearly distinct signal difference between promethazine-treated WT and 5XFAD mice after intravenous injection of the compound. Impressively, the inter-sample consistency of the promethazine-generated MALDI IMS signal facilitates 100% accurate discrimination of AD from WT mouse models using only a simple threshold analysis. Given the convergent evidence offered by MALDI IMS and corroborating HPLC data, we conclude that promethazine is retained in an amyloid-dependent manner in the brain. Moreover, regional differences in the retention of promethazine correlate well with the spatial distribution of Aβ plaques in the brain which further supports the conclusion that promethazine is capable of binding Aβ plaques. Overall, these findings support the specificity of promethazine for Aβ plaques and its potential utility in assessing AD plaque pathology. Increasing the plausibility of this conclusion, although identified as part of a random screening process, promethazine contains a unique structural scaffold which bears a striking resemblance to that of prototypical amyloid-binding compounds. For instance, while thioflavin exhibits a thiazole backbone, promethazine is supported by a phenothiazine structural motif. While the two backbone structures are different, they share common features including an N-alkylation extension from the ring system and a dimethyl amine moiety. However, critical structural differences between these compounds exist, which likely underlie promethazine's ability to cross the BBB. For example, the electronic neutrality of promethazine probably facilitates its penetrance into the CNS, while thioflavin's quaternary amine moiety imparts a positive charge which reduces its lipophilicity and thus negatively impacts its bio-distribution into the brain (Engkvist et al., 2003). Although independently confirmed in our work, we are keenly aware of promethazine's bio-distribution profile associated with its use as an antihistamine drug. Despite being aware of the well-established side-effect profile of promethazine and other first-generation antihistamines, a unique aspect of PET imaging probe development is that this technique uses a trace amount of radiolabeled compound, which is well below the threshold for inducing adverse pharmacological effects. Fortunately, the chemical structure of promethazine is quite unique relative to the development of a [^{11}C]carbon PET imaging probe via N-methylation using [^{11}C]methyl triflate or [^{11}C]methyl iodide (Nolting et al., 2012).

Table 1
MALDI IMS signals corresponding to $A\beta_{40}$ in the brains of 5XFAD mice.

Peptide	$[M + H]^+$average, predicted	$[M + H]^+$, observed
Aβ 1–37	4075.5	4076
Aβ 1–38	4132.6	4134
Aβ 1–39	4231.7	4232
Aβ 1–40	4330.9	4332

The advantage of this chemistry is that it retains the original chemical structure of the labeled compounds, thus minimizing the risk of binding affinity alterations or biodistribution at the target site. As stated, however, a number of caveats still await resolution. At present, for instance, we do not know the threshold at which we can distinguish the amyloid binding signal from the signal emitted upon binding to histamine receptors. Further, the binding affinity of promethazine to Aβ plaque is largely unknown, and that parameter is crucial to defining a PET probe. Notably, work is underway in our laboratory to address these issues.

5. Conclusions

We demonstrated a novel screening approach that facilitates the identification of amyloid-binding compounds and offers the potential for adaptation to a high-throughput platform. This approach differs from conventional probe discovery methodologies by extending beyond the in vitro binding affinity assay and offering information regarding a candidate probes performance in an in vivo model of AD. To facilitate this improvement, we utilize the 5XFAD model, combined with a robust mass spectrometry imaging capability. The MALDI IMS method combines the multichannel (m/z) measurement capability of mass spectrometry with a surface sampling process, enabling us to probe and map the presence of promethazine in the brain tissues (Cornett et al., 2007). In light of the substantial number of untested and orphaned compounds untested with respect to Aβ plaque affinity, we anticipate that this combinatorial approach to probe development will enhance the likelihood of getting a hit by facilitating rapid evaluation of untapped molecular libraries. Because of the operational simplicity, high sensitivity, compatibility with high-throughput platforms, it is our hope that the approach outlined in this work will serve to catalyze far-reaching advances in the development and understanding of AD pathophysiology, diagnostics and therapeutics.

Acknowledgments

We thank Meying Zhu for excellent technical assistance during the course of work. The work described was partially funded by the VICC Cancer Center Support Grants (W.P.), R01CA160700 (W.P.), 5R01GM058008-14 (R.M.C.) and P50CA128323 (J.C.G.).

Conflict of interest statement

The authors declare no competing financial interests.

Statement of provisional patent

Please note a provisional patent protecting the intellectual property outlined in this manuscript has been filed. This patent extends to the use of promethazine as a radiolabeled probe for amyloid imaging as well as structurally similar compounds.

Appendix A. Supplementary data

Supplementary data to this article can be found online at http://dx.doi.org/10.1016/j.nicl.2013.04.015.

References

Aisen, P., 2008. The plaque plan. Nature 456, 161–164.
Aisen, P.S., Vellas, B., 2013. Editorial: passive immunotherapy for Alzheimer's disease: what have we learned, and where are we headed? The Journal of Nutrition, Health & Aging 17, 49–50.
Albert, M.S., DeKosky, S.T., Dickson, D., Dubois, B., Feldman, H.H., Fox, N.C., Gamst, A., Holtzman, D.M., Jagust, W.J., Petersen, R.C., Snyder, P.J., Carrillo, M.C., Thies, B., Phelps, C.H., 2011. The diagnosis of mild cognitive impairment due to Alzheimer's disease: recommendations from the National Institute on Aging-Alzheimer's Association workgroups on diagnostic guidelines for Alzheimer's disease. Alzheimer's & Dementia 7, 270–279.
Allender, W.J., Archer, A.W., 1984. Liquid chromatographic analysis of promethazine and its major metabolites in human postmortem material. Journal of Forensic Sciences 29, 515–526.
Artero, S., Ritchie, K., 2003. The detection of mild cognitive impairment in the general practice setting. Aging & Mental Health 7, 251–258.
Artero, S., Tierney, M.C., Touchon, J., Ritchie, K., 2003. Prediction of transition from cognitive impairment to senile dementia: a prospective, longitudinal study. Acta Psychiatrica Scandinavica 107, 390–393.
Association, A.s., 2012. 2012 Alzheimer's disease facts and figures. Alzheimer's and Dementia: The Journal of the Alzheimer's Association 131–168.
Braak, H., Braak, E., 1995. Staging of Alzheimer's disease-related neurofibrillary changes. Neurobiology of Aging 16, 271–278 (discussion 278–284).
Choi, S.R., Golding, G., Zhuang, Z., Zhang, W., Lim, N., Hefti, F., Benedum, T.E., Kilbourn, M.R., Skovronsky, D., Kung, H.F., 2009. Preclinical properties of ^{18}F-AV-45: a PET agent for Abeta plaques in the brain. Journal of Nuclear Medicine 50, 1887–1894.
Cohen, A.D., Rabinovici, G.D., Mathis, C.A., Jagust, W.J., Klunk, W.E., Ikonomovic, M.D., 2012. Using Pittsburgh Compound B for in vivo PET imaging of fibrillar amyloid-beta. Advances in Pharmacology 64, 27–81.
Cornett, D.S., Reyzer, M.L., Chaurand, P., Caprioli, R.M., 2007. MALDI imaging mass spectrometry: molecular snapshots of biochemical systems. Nature Methods 4, 828–833.
Cummings, B.J., Cotman, C.W., 1995. Image analysis of beta-amyloid load in Alzheimer's disease and relation to dementia severity. The Lancet 346, 1524–1528.
Cummings, B.J., Pike, C.J., Shankle, R., Cotman, C.W., 1996. Beta-amyloid deposition and other measures of neuropathology predict cognitive status in Alzheimer's disease. Neurobiology of Aging 17, 921–933.
D'Amore, J.D., Kajdasz, S.T., McLellan, M.E., Bacskai, B.J., Stern, E.A., Hyman, B.T., 2003. In vivo multiphoton imaging of a transgenic mouse model of Alzheimer disease reveals marked thioflavine-S-associated alterations in neurite trajectories. Journal of Neuropathology and Experimental Neurology 62, 137–145.
de Souza, L.C., Lehericy, S., Dubois, B., Stella, F., Sarazin, M., 2012. Neuroimaging in dementias. Current Opinion in Psychiatry 25, 473–479.
Delrieu, J., Ousset, P.J., Caillaud, C., Vellas, B., 2012. 'Clinical trials in Alzheimer's disease': immunotherapy approaches. Journal of Neurochemistry 120 (Suppl. 1), 186–193.
Engkvist, O., Wrede, P., Rester, U., 2003. Prediction of CNS activity of compound libraries using substructure analysis. Journal of Chemical Information and Computer Sciences 43, 155–160.
Ghiso, J., Frangione, B., 2002. Amyloidosis and Alzheimer's disease. Advanced Drug Delivery Reviews 54, 1539–1551.
Glenner, G.G., Wong, C.W., 2012. Alzheimer's disease: initial report of the purification and characterization of a novel cerebrovascular amyloid protein. 1984 Biochemical and Biophysical Research Communications 425, 534–539.
Grundman, M., Pontecorvo, M.J., Salloway, S.P., Doraiswamy, P.M., Fleisher, A.S., Sadowsky, C.H., Nair, A.K., Siderowf, A., Lu, M., Arora, A.K., Agbulos, A., Flitter, M.L., Krautkramer, M.J., Sarsour, K., Skovronsky, D.M., Mintun, M.A., for the, A.V.A.S.G., 2013. Potential impact of amyloid imaging on diagnosis and intended management in patients with progressive cognitive decline. Alzheimer Disease and Associated Disorders 27, 4–15.
Hardy, J.A., Higgins, G.A., 1992. Alzheimer's disease: the amyloid cascade hypothesis. Science 256, 184–185.
Hardy, J., Selkoe, D.J., 2002. The amyloid hypothesis of Alzheimer's disease: progress and problems on the road to therapeutics. Science 297, 353–356.
Hintersteiner, M., Enz, A., Frey, P., Jaton, A.L., Kinzy, W., Kneuer, R., Neumann, U., Rudin, M., Staufenbiel, M., Stoeckli, M., Wiederhold, K.H., Gremlich, H.U., 2005. In vivo detection of amyloid-beta deposits by near-infrared imaging using an oxazine-derivative probe. Nature Biotechnology 23, 577–583.
Hort, J., O'Brien, J.T., Gainotti, G., Pirttila, T., Popescu, B.O., Rektorova, I., Sorbi, S., Scheltens, P., Dementia, E.S.P.o, 2010. EFNS guidelines for the diagnosis and management of Alzheimer's disease. European Journal of Neurology 17, 1236–1248.
Hudson, S.A., Ecroyd, H., Kee, T.W., Carver, J.A., 2009. The thioflavin T fluorescence assay for amyloid fibril detection can be biased by the presence of exogenous compounds. FEBS Journal 276, 5960–5972.
Ikonomovic, M.D., Abrahamson, E.E., Price, J.C., Hamilton, R.L., Mathis, C.A., Paljug, W.R., Debnath, M.L., Cohen, A.D., Mizukami, K., DeKosky, S.T., Lopez, O.L., Klunk, W.E., 2012. Early AD pathology in a [C-11]PiB-negative case: a PiB-amyloid imaging, biochemical, and immunohistochemical study. Acta Neuropathologica 123, 433–447.
Jack Jr., C.R., Petersen, R.C., Xu, Y.C., O'Brien, P.C., Smith, G.E., Ivnik, R.J., Boeve, B.F., Waring, S.C., Tangalos, E.G., Kokmen, E., 1999. Prediction of AD with MRI-based hippocampal volume in mild cognitive impairment. Neurology 52, 1397–1403.
Kerchner, G.A., 2011. Ultra-high field 7 T MRI: a new tool for studying Alzheimer's disease. Journal of Alzheimer's Disease 26 (Suppl. 3), 91–95.
Klunk, W.E., Engler, H., Nordberg, A., Wang, Y., Blomqvist, G., Holt, D.P., Bergstrom, M., Savitcheva, I., Huang, G.F., Estrada, S., Ausen, B., Debnath, M.L., Barletta, J., Price, J.C., Sandell, J., Lopresti, B.J., Wall, A., Koivisto, P., Antoni, G., Mathis, C.A., Langstrom, B., 2004. Imaging brain amyloid in Alzheimer's disease with Pittsburgh Compound-B. Annals of Neurology 55, 306–319.
Klunk, W.E., Price, J.C., Mathis, C.A., Tsopelas, N.D., Lopresti, B.J., Ziolko, S.K., Bi, W., Hoge, J.A., Cohen, A.D., Ikonomovic, M.D., Saxton, J.A., Snitz, B.E., Pollen, D.A., Moonis, M., Lippa, C.F., Swearer, J.M., Johnson, K.A., Rentz, D.M., Fischman, A.J., Aizenstein, H.J., DeKosky, S.T., 2007. Amyloid deposition begins in the striatum of presenilin-1 mutation carriers from two unrelated pedigrees. Journal of Neuroscience 27, 6174–6184.
Koffie, R.M., Farrar, C.T., Saidi, L.J., William, C.M., Hyman, B.T., Spires-Jones, T.L., 2011. Nanoparticles enhance brain delivery of blood–brain barrier-impermeable probes for in vivo optical and magnetic resonance imaging. Proceedings of the National Academy of Sciences of the United States of America 108, 18837–18842.

Kumagai, H., Pham, W., Kataoka, M., Hiwatari, K.I., McBride, J., Wilson, K.J., Tachikawa, H., Kimura, R., Nakamura, K., Liu, E.H., Gore, J.C., Sakuma, S., 2012. Multifunctional nanobeacon for imaging Thomsen–Friedenreich antigen-associated colorectal cancer. International Journal of Cancer 132, 2107–2117.

Landau, S.M., Harvey, D., Madison, C.M., Koeppe, R.A., Reiman, E.M., Foster, N.L., Weiner, M.W., Jagust, W.J., Alzheimer's Disease Neuroimaging, I., 2011. Associations between cognitive, functional, and FDG-PET measures of decline in AD and MCI. Neurobiology of Aging 32, 1207–1218.

Landau, S.M., Mintun, M.A., Joshi, A.D., Koeppe, R.A., Petersen, R.C., Aisen, P.S., Weiner, M.W., Jagust, W.J., Alzheimer's Disease Neuroimaging, I., 2012. Amyloid deposition, hypometabolism, and longitudinal cognitive decline. Annals of Neurology 72, 578–586.

Lansbury Jr., P.T., 2004. Back to the future: the 'old-fashioned' way to new medications for neurodegeneration. Nature Medicine 10, S51–S57 (Suppl.).

LeVine III, H., 1993. Thioflavine T interaction with synthetic Alzheimer's disease beta-amyloid peptides: detection of amyloid aggregation in solution. Protein Science 2, 404–410.

Lewis, J., Dickson, D.W., Lin, W.L., Chisholm, L., Corral, A., Jones, G., Yen, S.H., Sahara, N., Skipper, L., Yager, D., Eckman, C., Hardy, J., Hutton, M., McGowan, E., 2001. Enhanced neurofibrillary degeneration in transgenic mice expressing mutant tau and APP. Science 293, 1487–1491.

Markesbery, W.R., 1999. The role of oxidative stress in Alzheimer disease. Archives of Neurology 56, 1449–1452.

Masters, C.L., Multhaup, G., Simms, G., Pottgiesser, J., Martins, R.N., Beyreuther, K., 1985a. Neuronal origin of a cerebral amyloid: neurofibrillary tangles of Alzheimer's disease contain the same protein as the amyloid of plaque cores and blood vessels. EMBO Journal 4, 2757–2763.

Masters, C.L., Simms, G., Weinman, N.A., Multhaup, G., McDonald, B.L., Beyreuther, K., 1985b. Amyloid plaque core protein in Alzheimer disease and Down syndrome. Proceedings of the National Academy of Sciences of the United States of America 82, 4245–4249.

Mathis, C.A., Mason, N.S., Lopresti, B.J., Klunk, W.E., 2012. Development of positron emission tomography beta-amyloid plaque imaging agents. Seminars in Nuclear Medicine 42, 423–432.

Meda, L., Cassatella, M.A., Szendrei, G.I., Otvos Jr., L., Baron, P., Villalba, M., Ferrari, D., Rossi, F., 1995. Activation of microglial cells by beta-amyloid protein and interferon-gamma. Nature 374, 647–650.

Merlini, G., Bellotti, V., 2003. Molecular mechanisms of amyloidosis. The New England Journal of Medicine 349, 583–596.

Mintun, M.A., Larossa, G.N., Sheline, Y.I., Dence, C.S., Lee, S.Y., Mach, R.H., Klunk, W.E., Mathis, C.A., DeKosky, S.T., Morris, J.C., 2006. [11C]PIB in a nondemented population: potential antecedent marker of Alzheimer disease. Neurology 67, 446–452.

Nesterov, E.E., Skoch, J., Hyman, B.T., Klunk, W.E., Bacskai, B.J., Swager, T.M., 2005. In vivo optical imaging of amyloid aggregates in brain: design of fluorescent markers. Angewandte Chemie (International Ed. in English) 44, 5452–5456.

Niessen, W.M., 2011. Fragmentation of toxicologically relevant drugs in positive-ion liquid chromatography–tandem mass spectrometry. Mass Spectrometry Reviews 30, 626–663.

Nolting, D.D., Gore, J.C., Pham, W., 2011. NEAR-INFRARED DYES: probe development and applications in optical molecular imaging. Current Organic Synthesis 8, 521–534.

Nolting, D.D., Nickels, M.L., Guo, N., Pham, W., 2012. Molecular imaging probe development: a chemistry perspective. American Journal of Nuclear Medicine and Molecular Imaging 2, 273–306.

Oakley, H., Cole, S.L., Logan, S., Maus, E., Shao, P., Craft, J., Guillozet-Bongaarts, A., Ohno, M., Disterhoft, J., Van Eldik, L., Berry, R., Vassar, R., 2006. Intraneuronal beta-amyloid aggregates, neurodegeneration, and neuron loss in transgenic mice with five familial Alzheimer's disease mutations: potential factors in amyloid plaque formation. Journal of Neuroscience 26, 10129–10140.

O'Keefe, G.J., Saunder, T.H., Ng, S., Ackerman, U., Tochon-Danguy, H.J., Chan, J.G., Gong, S., Dyrks, T., Lindemann, S., Holl, G., Dinkelborg, L., Villemagne, V., Rowe, C.C., 2009. Radiation dosimetry of beta-amyloid tracers ^{11}C-PiB and ^{18}F-BAY94-9172. Journal of Nuclear Medicine 50, 309–315.

Perrin, R.J., Fagan, A.M., Holtzman, D.M., 2009. Multimodal techniques for diagnosis and prognosis of Alzheimer's disease. Nature 461, 916–922.

Petersen, R.C., Doody, R., Kurz, A., Mohs, R.C., Morris, J.C., Rabins, P.V., Ritchie, K., Rossor, M., Thal, L., Winblad, B., 2001. Current concepts in mild cognitive impairment. Archives of Neurology 58, 1985–1992.

Ponder, G.W., Stewart, J.T., 1995. A liquid chromatographic method for the determination of promethazine enantiomers in human urine and serum using solid-phase extraction and fluorescence detection. Journal of Pharmaceutical and Biomedical Analysis 13, 1161–1166.

Prince, M., Bryce, R., Ferri, C., 2011. The benefits of early diagnosis and intervention. Alzheimer's Disease International, World Alzheimer Report Institute of Psychiatry, King's College London, p. 4.

Risacher, S.L., Saykin, A.J., 2013. Neuroimaging and other biomarkers for Alzheimer's disease: the changing landscape of early detection. Annual Review of Clinical Psychology 9, 621–648.

Ritchie, K., Ancelin, M.L., Beaino, E., Portet, F., Brickman, A.M., Dartigues, J.F., Tzourio, C., Dupuy, A.M., Ritchie, C.W., Berr, C., Artero, S., 2010. Retrospective identification and characterization of mild cognitive impairment from a prospective population cohort. The American Journal of Geriatric Psychiatry 18, 692–700.

Rosenberg, R.N., 2005. Translational research on the way to effective therapy for Alzheimer disease. Archives of General Psychiatry 62, 1186–1192.

Seeley, E.H., Caprioli, R.M., 2008. Molecular imaging of proteins in tissues by mass spectrometry. Proceedings of the National Academy of Sciences of the United States of America 105, 18126–18131.

Selkoe, D.J., 1991a. Alzheimer's disease. In the beginning. Nature 354, 432–433.

Selkoe, D.J., 1991b. Amyloid protein and Alzheimer's disease. Scientific American 265, 68–71 (74-66, 78).

Sheng, J.G., Mrak, R.E., Griffin, W.S., 1997. Glial-neuronal interactions in Alzheimer disease: progressive association of IL-1alpha+ microglia and S100beta+ astrocytes with neurofibrillary tangle stages. Journal of Neuropathology and Experimental Neurology 56, 285–290.

Sorbi, S., Hort, J., Erkinjuntti, T., Fladby, T., Gainotti, G., Gurvit, H., Nacmias, B., Pasquier, F., Popescu, B.O., Rektorova, I., Religa, D., Rusina, R., Rossor, M., Schmidt, R., Stefanova, E., Warren, J.D., Scheltens, P., Dementia, E.S.P.o, Cognitive, N., 2012. EFNS-ENS Guidelines on the diagnosis and management of disorders associated with dementia. European Journal of Neurology 19, 1159–1179.

Terry, R.D., Katzman, R., 1983. Senile dementia of the Alzheimer type. Annals of Neurology 14, 497–506.

Van Heertum, R.L., Tikofsky, R.S., 2003. Positron emission tomography and single-photon emission computed tomography brain imaging in the evaluation of dementia. Seminars in Nuclear Medicine 33, 77–85.

Villemagne, V.L., Ong, K., Mulligan, R.S., Holl, G., Pejoska, S., Jones, G., O'Keefe, G., Ackerman, U., Tochon-Danguy, H., Chan, J.G., Reininger, C.B., Fels, L., Putz, B., Rohde, B., Masters, C.L., Rowe, C.C., 2011. Amyloid imaging with (18)F-florbetaben in Alzheimer disease and other dementias. Journal of Nuclear Medicine 52, 1210–1217.

Voropai, E.S., Samtsov, M.P., Kaplevskii, K.N., Maskevich, A.A., Stepuro, V.I., Povarova, O.I., Kuznetsova, I.M., Turoverov, K.K., Fink, A.L., Uverskii, V.N., 2003. Spectral properties of thioflavin T and its complexes with amyloid fibrils. Journal of Applied Spectroscopy 70, 868–874.

Wang, P.N., Lirng, J.F., Lin, K.N., Chang, F.C., Liu, H.C., 2006. Prediction of Alzheimer's disease in mild cognitive impairment: a prospective study in Taiwan. Neurobiology of Aging 27, 1797–1806.

Weiner, M.W., Veitch, D.P., Aisen, P.S., Beckett, L.A., Cairns, N.J., Green, R.C., Harvey, D., Jack, C.R., Jagust, W., Liu, E., Morris, J.C., Petersen, R.C., Saykin, A.J., Schmidt, M.E., Shaw, L., Siuciak, J.A., Soares, H., Toga, A.W., Trojanowski, J.Q., Alzheimer's Disease Neuroimaging, I., 2012. The Alzheimer's disease neuroimaging initiative: a review of papers published since its inception. Alzheimer's & Dementia 8, S1–S68.

Yanagisawa, D., Amatsubo, T., Morikawa, S., Taguchi, H., Urushitani, M., Shirai, N., Hirao, K., Shiino, A., Inubushi, T., Tooyama, I., 2011. In vivo detection of amyloid beta deposition using (1)(9)F magnetic resonance imaging with a (1)(9)F-containing curcumin derivative in a mouse model of Alzheimer's disease. Neuroscience 184, 120–127.

Zhang, S., Han, D., Tan, X., Feng, J., Guo, Y., Ding, Y., 2012. Diagnostic accuracy of 18 F-FDG and 11 C-PIB-PET for prediction of short-term conversion to Alzheimer's disease in subjects with mild cognitive impairment. International Journal of Clinical Practice 66, 185–198.